Received: 23 March 2016 | Revised: 26 September 2016 | Accepted: 21 October 2016

DOI: 10.1002/cnm.2844

WILEY

RESEARCH ARTICLE

Automated femoral landmark extraction for optimal prosthesis placement in total hip arthroplasty

Diogo F. de Almeida[1,2] | Rui B. Ruben[3] | João Folgado[1] | Paulo R. Fernandes[1] | João Gamelas[4] | Benedict Verhegghe[2] | Matthieu De Beule[2]

[1]IDMEC, Instituto Superior Técnico, Universidade de Lisboa, Lisbon, Portugal
[2]IBiTech-bioMMeda, Ghent University, Ghent, Belgium
[3]ESTG, CDRSP, Polytechnic Institute of Leiria, Leiria, Portugal
[4]Medical School, Universidade Nova de Lisboa, Lisbon, Portugal

Correspondence
Diogo Ferreira de Almeida, IDMEC, Instituto Superior Técnico, Av. Rovisco Pais, 1, 1049-001 Lisboa, Portugal.
Email: diogo@dem.ist.utl.pt

Funding information
FEDER/COMPETE; Portuguese Foundation for Science and Technology (FCT), Grant/Award Number: PTDC/SAU-BEB/103408/2008, SFRH/BD/71822/2010; IDMEC/LAETA, Grant/Award Number: UID/EMS/50022/2013

Abstract

The automated extraction of anatomical reference landmarks in the femoral volume may improve speed, precision, and accuracy of surgical procedures, such as total hip arthroplasty. These landmarks are often hard to achieve, even via surgical incision. In addition, it provides a presurgical guidance for prosthesis sizing and placement. This study presents an automated workflow for femoral orientation and landmark extraction from a 3D surface mesh. The extraction of parameters such as the femoral neck axis, the femoral middle diaphysis axis, both trochanters and the center of the femoral head will allow the surgeon to establish the correct position of bony cuts to restore leg length and femoral offset. The definition of the medullary canal endosteal wall is used to position the prosthesis' stem. Furthermore, prosthesis alignment and sizing methods were implemented to provide the surgeon with presurgical information about performance of each of the patient-specific femur-implant couplings. The workflow considers different commercially available hip stems and has the potential to help the preoperative planning of a total hip arthroplasty in an accurate, repeatable, and reliable way. The positional and orientation errors are significantly reduced, and therefore, the risk of implant failure and subsequent revision surgery are also reduced.

KEYWORDS

3D landmark extraction, 3D surface mesh, computed tomography, hip prosthesis, preoperative planning, total hip arthroplasty

1 | INTRODUCTION

Even though the total hip arthroplasty (THA) surgical procedure is considered to be among the most successful, safe, and cost-effective surgical procedures, implant failures related to prosthesis design and placement still occur in a considerable number.[1] The absence of reliable landmarks defining the alignment of the femur and pelvis and restricted accessibility makes the placement of the hip implant more difficult during surgery. Hence, a proper planning of the surgical procedure on the basis of patient-specific image processing will reduce the intraoperative risk of human error and consequently increase the durability of the implant.[2] Moreover, the automation of such methods will thoroughly improve the surgical planning experience and will ultimately decrease the time of the surgical procedure and risk of unexpected complications.

The durability of the implant is determined by its interaction with the bone tissue, which is a complex, continuously evolving structure. The femoral anatomy differs in anteversion angle, anterolateral bowing of the femur and neck-shaft angle between individuals. The knowledge of this anatomy may help to reduce the high incidence of implant dislocation.[3] Moreover, clinical and experimental studies have demonstrated that a close geometric fit between the femoral component and supporting bone is essential for durable implant fixation.[4] Therefore, it is safe to assume that the success of THA is critically related to the knowledge of the femur geometry and the predictability of the key femoral dimensions. These two allow the optimization of the design and placement

of hip implants in the femur for a better coupling. Consequently, the design and the prosthesis placement can provide a load transmission system that optimizes the longevity of the implant.

Patient-specific modeling from image datasets is recognized as the gold-standard technique to computationally represent the hip joint in preoperative planning, although it can be susceptible to slight error variations.[5] Classic techniques such as 2D templating lack in repeatability and 3D insight of the anatomy, ie, anteroposterior and lateral radiographies merely provide one projection of the pelvis and the femur, and therefore, one of the dimensions is lost in the acquisition. Computed tomography (CT) scans allow the visualization of the hip joint anatomy in 3 dimensions and consequently plan the implantation of the femoral and acetabular components with superior accuracy. In addition, recent developments in image acquisition techniques with special low-dose CT scan protocols are being presented,[6–8] which reduces significantly the radiation exposure of the patients. This way, restoration of leg length, center of rotation, range of motion of the joint, and points of bony and prosthetic impingement can be analyzed preoperatively by the surgeon.[9]

When computationally recreating an anatomical environment, the identification and location of prominent features of the organism as reference parameters, such as distances of angles, is of great utility: they can be helpful for objective diagnosis purposes,[10,11] preoperative planning,[11–13] computer aided surgery,[14,15] and postoperative follow-up.[16,17] Manual landmark extraction is time consuming, and its repeatability and accuracy rely on the level of expertise of the observer. Later, a semi-automatic landmark detection on the basis of the local curvature of isocontours initiated manually was proposed.[18] More recently, fully automatic landmark detection methods on the basis o statistical models[19,20] were also proposed. These methods are more prone to accuracy errors, because of their dependency on the population size of the trained model. In addition, the training of this model can be very time consuming. Pure geometric analysis methods achieve high reproductibility and are computationally less expensive when compared to their alternatives, although they highly depend on the level of discretization of the surface mesh.[21]

Within this context, a set of tools to properly plan the THA on the basis of the landmark extraction of the hip joint was developed under pyFormex,* which is an open-source program under development at IBiTech-bioMMeda that provides a wide range of operations for generating, transforming, and manipulating surface meshes. Its aims are not only at an improved alignment of the hip prosthesis but also to provide instant information and feedback to the surgeon, which may make the surgical technique easier to perform leading to better prosthetic positioning.

*http://www.nongnu.org/pyformex/

The toolbox automatically extracts femoral landmarks and measurements from a triangular surface mesh over which the prosthesis placement is planned. For instance, with the definition of the femoral neck axis (FNA) and the femoral middle diaphysis axis (FMDA), it is possible to promptly infer the femoral angle of anteversion and neck-shaft angle and diagnose excessive retroversion or anteversion, as well as above normal femoral neck angles. In addition, these axis allow an ideal presurgical alignment of the prosthesis' stem and neck. Landmarks such as the greater and lesser trochanters or the saddle point of the femoral neck allow improvements in the osteotomy planning, such that the amount of bone mass removed is minimized. The definition of the femur medullary canal and the knowledge of its endosteal's anatomy allows prosthesis sizing and ultimately reduces the unnecessary broaching of the cavity for prosthesis fixation. The sizing of the implant can be such that maintains the anatomical leg length and femoral offset.

In summary, the toolbox presented here allows the surgeon to better plan the patient-specific THA without the knowledge of the techniques used behind the methods. Combining a 3D reconstructed surface mesh of the femur with a set of commercially available implants, the planning presented here will reduce the surgical time and cost. Three-dimensional finite element meshes can be generated of the femur-implant coupling, and the performances of different implant sizes and designs can be compared preoperatively.

2 | MATERIALS AND METHODS

2.1 | Bone models

The methodology presented in this work was developed using segmented femurs from CT scan images using a fully automatic, active shape model–based algorithm[22] and then importing them into pyFormex. The segmentation of the medullary cavity of each femur was also performed. For the shape model training, high resolution images acquired at the Ghent University Hospital, in Belgium, were used. The training images averaged a 0.666 ± 0.069 mm $\times$ 0.666 ± 0.069 mm pixel resolution and a 0.6 mm slice increment, which allowed the shape model segmentation a robust and accurate performance even in low quality, clinical practice CT scans.[22]

The database is heterogeneous, containing normal and injured pelves or femurs of THA candidates. However, specimens with metallic implants, abnormal bone formations, severe osteoporosis, or partially occluded femurs were excluded. The sample group consisted of 50 individuals, 25 of each sex. The average age of the male individuals was 64.7 ± 13.6 years while for the female individuals it was 71.7 ± 14.4 years. The combined average age was 67.7 ± 14.3 years.

2.2 | Standardized coordinate system

The presented feature extraction process is invariant to the orientation of the bone. Therefore, to standardize the coordinate system for the complete femur, the origin and a system of axes that is common to all femurs has to be defined. To do so, the affine transformation matrix that transfers the femur from the CT image coordinates to the new standardized coordinate system is calculated and applied to the femur in the CT image coordinates, ie, so that any translational and rotational variations are removed.

The first step of the alignment is to determinate the center of gravity (C) of the surface mesh and set it as the origin. Then, the calculation of the principal axes of inertia of the outer surface estimates the anteroposterior, right-left, and distoproximal (DP) directions of the femur. A workflow on the basis of volumetric splitting and part size comparison[13] was established to classify the femur as right or left. An example of a surface mesh translated to the origin and without any rotational variation is shown in Figure 1. The definition of such a coordinate system proved to be of added value to the extraction of the anatomical landmarks of the femur and geometrical entities fitting, as relative positioning can be assumed a priori.

2.3 | Femoral middle diaphysis axis and intramedullary axis

The FMDA is defined as the straight axis of the femoral diaphysis or shaft. It is computed firstly by clipping the surface along DP, ie, symmetric around the origin, over a height that is equal to half of the femoral length along the DP direction. Then, a circle is fitted to the points of each cross section boundary and the centroid point is calculated. The FMDA is then calculated by defining the covariance matrix Σ of the mean-centered data points X,

$$\Sigma = \frac{X^{\mathrm{T}}X}{m} \tag{1}$$

where m is the number of points, and performing singular value decomposition on Σ. This will return the direction vector of the line that best fits FMDA in the least squares sense as the first principal component. Figure 2 shows an example of the estimated FMDA for the human femur.

However, due to the medullary cavity present on the femur, to define the FMDA as the ideal prosthesis insertion axis may result in unnecessary cavity reaming, ie, excessive removal of cortical bone on the inner wall of the femoral shaft. This will ultimately result in a decreased femoral shaft load-bearing capacity. Hence, an estimate of the intramedullary axis was

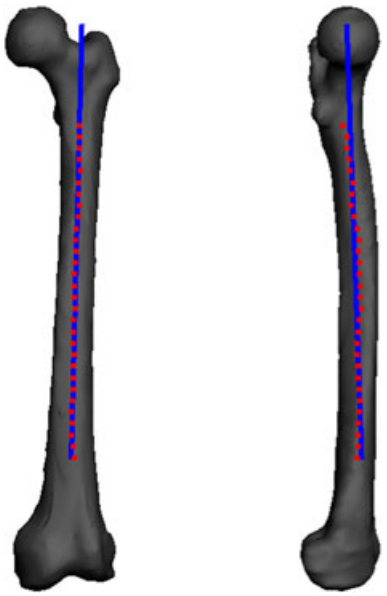

FIGURE 2 Anterior and lateral views of the femoral middle diaphysis axis. The axis (in blue) is determined by a linear regression on the medial points (in red) of the centroids obtained by cross sectioning the femoral shaft along the inferior-superior direction

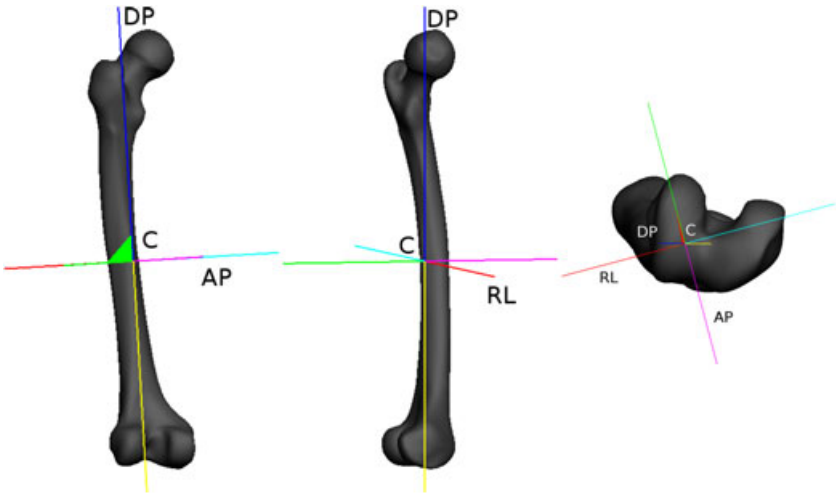

FIGURE 1 Principal axes of inertia of a femur model, respectively, frontal, lateral, and bottom views. For labeling simplifications, the right-left, anteroposterior, and distoproximal axes will be respectively referred to as x, y, and z

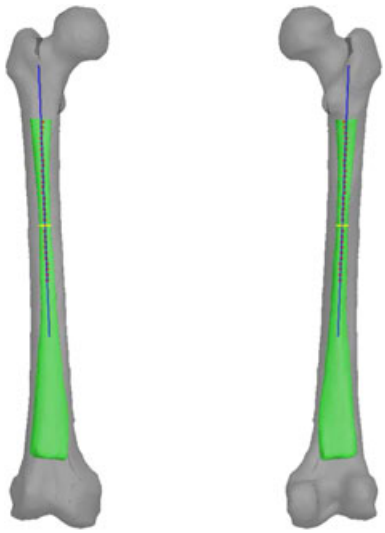

FIGURE 3 Anterior and posterior views of the prosthesis insertion axis and the cavity isthmus. The axis (in blue) is determined by a linear regression on the medial points (in red) of the medullary canal (in green). The isthmus (in yellow) is defined as the minimum cross-sectional area of the cutting planes along the prosthesis insertion axis

estimated, on the basis of the same pipeline as the FMDA, and defined as the prosthesis insertion axis. In addition, the medullary isthmus, which is defined as the smallest cross-sectional area in the medullary cavity, is also extracted for prosthesis placement purposes. Figure 3 illustrates both the intramedullary axis and the isthmus of a femur. The position of the isthmus is highly variable, and if located too superiorly, it may require intramedullary reaming to adapt the canal to the prosthesis stem design.

2.4 | Femoral neck axis and head center extraction

In addition to the prosthesis' stem insertion axis, the computational estimation of the FNA is also important to try to optimize the prosthesis placement in preoperative planning. The CT scan is considered as accurate and reliable as gold-standard techniques for locating the femoral head center because of its 3D nature.[23]

The FNA is defined by the line that connects the center of the head of the femur and the centroid of the smallest cross section on the neck of the femur. The cross-sectional area depends on the position and orientation of the slicing plane. Therefore, and on the basis of the standardized coordinate system defined in the previous subsection, the neck was sliced along a normal with coordinates (1,0,1). Each slicing of the mesh will result in a polygon defined by P_i vertices and its area can be computed using

$$A = \boldsymbol{n} \cdot \sum_{i=0}^{N-1} \frac{P_i \times P_{i+1}}{2} \tag{2}$$

where $\boldsymbol{n}$ is the normal to the plane containing the polygon and N is the number of points on the border of the polygon.

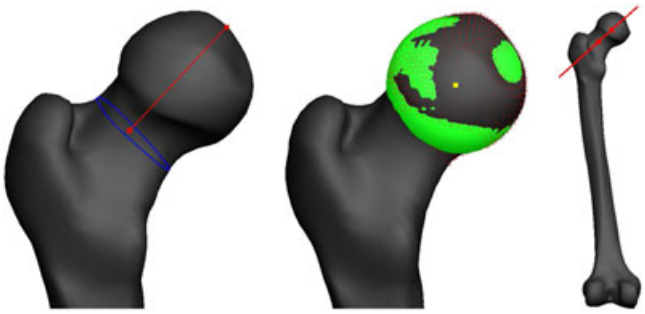

FIGURE 4 Posterior view of the proximal femur. On the left, the smallest cross section of the femoral neck is shown in blue. The red line shows the normal vector of the slicing plane, positioned at the center of the cross section. On the center, the sphere fitted to the femoral head is shown in green. The red lines show the normal of the vertices considered for the fitting and the yellow mark at the center of the femoral head represents the geometrical center of the fitted sphere, also assumed the center of the femoral head. On the right, the femoral neck axis is shown in red

From here, we can obtain the smallest cross section along the femoral neck. Figure 4 (left) shows the cross section on the neck of the femur considered to be the smallest and the normal used to estimate the slicing planes.

The center of the head of the femur is estimated by fitting a parametric spherical surface to the partial sphere defined by the head of the femur. For that, the proximal femur is sectioned again perpendicularly to the normal defined before and the relative difference in the sectional area allows the estimation of the nodes in the mesh that define the femoral head. Then, a quartic surface is fitted to those nodes of the triangular mesh and a well-approximated femoral head is obtained. Figure 4 (center) shows the best fitting sphere to the femoral head vertices, whose normals are represented in red.

The axis defined by the center of the smallest cross section and the center of the head defines the FNA. Together with the FMDA, it allows us to calculate the femoral neck-shaft angle if measured in the coronal plane (see Section 2.7). Moreover, combined with the prosthesis insertion axis, it will be used to better plan the prosthesis placement. Also in Figure 4 (right), the FNA is represented in a generic femur mesh.

2.5 | Greater and lesser trochanters

Proximal femoral resection is the surgical removal of the femoral head and part of the proximal femur. This is done in case of injury and to replace the hip joint. The portion of removed femur depends on the lesion of the femur. Therefore, the femur osteotomy location and cutting plane are planned so that the portion of removed femur is minimized. To locate and position the femoral osteotomy, pipelines for the automatic detection of both femoral trochanters were implemented.

Again taking advantage of the standardized coordinate system defined in Section 2.2, the extraction of both the greater and the lesser trochanter was based on volume sectioning along their normal. Its accuracy depends on the level of

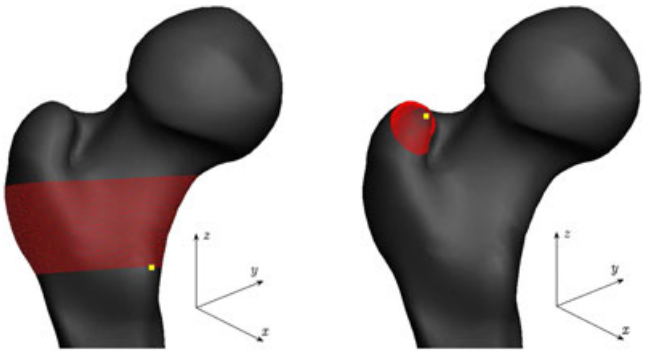

FIGURE 5 Lesser (left) and greater (right) femoral trochanters shown in yellow. The extraction algorithm starts in an automatically predicted point and segments the surface mesh perpendicularly to a given normal as shown in red. The normals are $\boldsymbol{n} = (0, 0, -1)$ for the lesser trochanter (left) and $\boldsymbol{n} = (1, 0, 1)$ for the greater trochanter (right)

discretization of the mesh and the size of the triangle faces of the mesh. Nevertheless, a mesh refinement proved to compensate accuracy of the method at the cost of an additional computational time.

For convex or concave structures, the extreme point along one direction is computed as the mesh vertex for which the length of the projection on the direction vector is maximal. As shown in Figure 5, the mesh was sectioned perpendicularly to an approximated direction of the normal to the mesh on the saddle point and the maximum value of the centroids of the sections in red is assumed to be the point of interest. The search process initiates in the center of gravity of the proximal femur. Expected curvature variances define the iterative algorithm's convergence criteria. Both trochanters are shown in yellow.

On the left of Figure 5, the largest axis of inertia was chosen as the normal of the iterative slicing plane and the algorithm looked for the maximum x value. Similarly, on the right, the greater trochanter extraction. The initial direction for the normal of the slicing plane was chosen as $\boldsymbol{n} = (1,0,1)$, which is roughly the direction of the FNA. However, the resulting section can have 2 islands: one formed by the trochanter and another by the neck of the femur. Due to this fact, the algorithm will assume that the one with smaller area corresponds to the greater trochanter.

2.6 | Neck saddle point

The extraction of neck saddle point is due to properly plan the osteotomy. Due to the saddle-shaped nature of the femoral neck, its curvature is different according to the direction considered. Therefore, and taking advantage of standardized coordinate system, the neck saddle point was considered to be the closest point to the FNA. Its location is straightforward as it will be the point with the maximum value in the z axis on the minimum cross-sectional perimeter of consecutive slices of the femoral neck perpendicular to the FNA. The neck saddle point is shown in Figure 6.

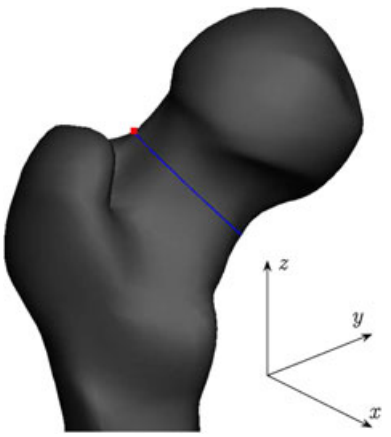

FIGURE 6 Extraction of the femoral neck saddle point. The minimal femoral neck cross-sectional perimeter is shown in blue and the neck saddle point, shown in red, is considered to be the point with the highest value in the z axis

2.7 | Femoral neck-shaft angle and anteversion angle

The landmark extraction and axis definition allows the calculation of the femoral neck-shaft angle and the femoral anteversion angle. The first is defined as the interior angle between the FMDA and the FNA and is used to diagnose the occurrence of coxa vara and coxa valga. It can vary within normality values between 126° and 139°. In the presence of an increased neck-shaft angle (equal or superior to 140°) or a decreased neck-shaft angle (equal or inferior to 125°), respectively, coxa valga and coxa vara, it can cause hip pain and degeneration. There are implants that compensate for these deviations to maintain equal leg length and femoral offset. Figure 7 features a visual representation of the neck-shaft angle.

The anteversion angle is used to measure the femoral torsion along its shaft. It can be defined as the angle between the condylar axis and the FNA, which is undetectable in 2 dimension radiographs. Normal version is a forward angle of 12° and 15°. In individuals with version abnormalities, the femoral neck may be rotated either too far forward (excessive anteversion) or too far backward (retroversion). These conditions result in the ball portion of the hip joint being situated at an unhealthy angle to the cup portion of the socket and can lead to damage to the hip joint surfaces and surrounding structures. Figure 7 also shows an example of the anteversion angle measurement in 3 dimensions.

2.8 | Osteotomy

Osteotomy is the surgical act of cutting a bone to shorten or lengthen it, to realign it. It is often used to correct bone deformities, straighten a bone that has healed crookedly following a fracture or to replace part of the bone by an implant. It is a significantly invasive procedure, and therefore, the recovery may be extensive. Femoral osteotomies are part of the THA procedure. Intuitively, the ideal situation would involve

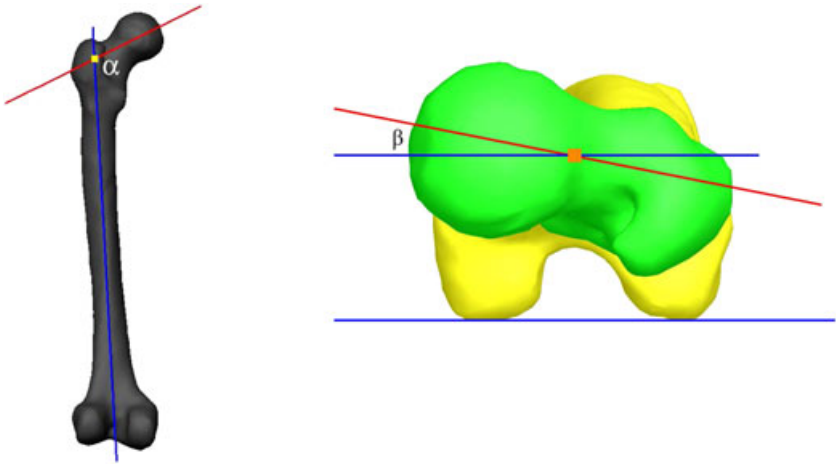

FIGURE 7 On the left, the femoral neck-shaft angle α is represented. It is the angle around the yellow intersection point of the FNA (in red) and the FMDA (in blue). This measure is clinically relevant as it denotes coxa vara and coxa valga abnormalities. On the right, the anteversion angle β is shown. It is the angle between the condylar axis (also in blue) and the FNA (in red). For visualization purposes, the proximal femur is represented in green and the femoral shaft and distal femur in yellow

the minimal bone mass removal for the prosthesis insertion, hence resulting from a higher femoral neck incision, which gives a better rotational stability to the stem. There are several approaches to make room for the prosthesis insertion, which depend mainly on the location and extension of the injury, the design of the implant, and the bone mass quality of the patient. Our experienced orthopedic partners consider that, ideally

1. The cutting plane should be approximately perpendicular to the axis of the femoral neck;
2. In general, the osteotomy should be performed about 2 cm proximal to the lesser trochanter, to, together with leg length and global offset, avoid inappropriate muscle tension.

An automated osteotomy reference plane is defined as perpendicular to the axis of the femoral neck and containing the neck saddle point. The femoral offset is defined as the perpendicular distance between the anatomical center of the femoral head to the intramedullary axis as projected onto the coronal plane, as shown in Figure 8 (left). Changes in the postsurgical femoral offset may reflect in a defective patient gait cycle and consequent limb pain.[24]

The neck osteotomy plane should be planned according to the implant's design. Moreover, femoral neck fractures occur in distinct regions of the neck, eg, subcapital or transcervical fractures. There are also often undetected bone tissue lesions during the automatic segmentation algorithms, which can also have direct influence on the osteotomy location. Hence, the developed framework is able to perform the osteotomy on the basis of the deviance in distance to the saddle point and in angle to the perpendicular plane of the FNA, which can be defined by the surgeon. At any instance, the user can check whether the distance to any of the trochanters is enough to avoid insufficient muscle tension. Nevertheless, whatever the planned osteotomy is, changes on the femoral offset can be compensated with prosthesis sizing and placement, which will be looked into in Section 2.10.

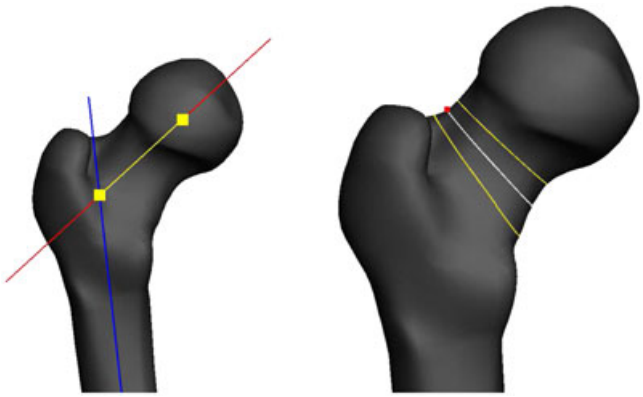

FIGURE 8 Posterior views of the proximal femur. On the left, the femoral offset (in yellow) is defined as the distance along the femoral neck axis (in red) between the anatomical center of the femoral head and its intersection with the intramedullary axis (in blue). The limits of the femoral offset are also shown in yellow. On the right, 3 planned osteotomy cutting planes are visible. As a reference, the saddle point of the femoral neck (in red) and the cutting plane perpendicular to the femoral neck axis (in white). The cutting planes shown in yellow are 2 cm deviated from the saddle point in both senses of the left-right direction and their normal is 6 degrees deviated from the reference cutting plane, respectively

Figure 8 (right) shows the reference cutting plane that passes through the femoral neck saddle point and is perpendicular to the femoral neck axis in white. Depending on several parameters, the cutting plane may vary its position and angle according to the user. To simplify the planning, this variation is translated in deviation to the reference plane and can be user defined. Also in Figure 8 (right), in yellow, other planes equidistant from the reference plane in opposite directions and whose cutting plane normal is equally deviated from the femoral neck axis in opposite directions are also shown as examples of the implementation.

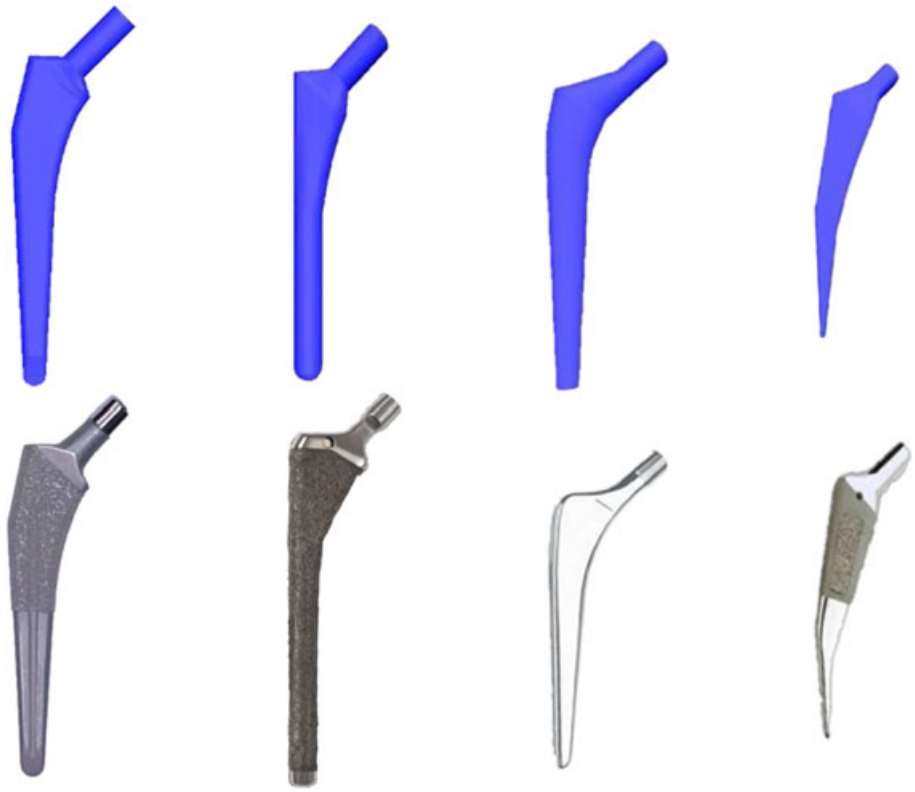

FIGURE 9 From left to right, DePuy Synthes TRI-LOCK® Bone Preservation Stem, the Zimmer® VerSys Epoch® FullCoat Hip System, the Zimmer® MS-30™stem and the Zimmer® Mayo® Conservative Hip Prosthesis. The first row shows the computational models of the prosthesis and the second row shows their corresponding real aspect

As the intention is to remove as less bone mass as possible, the osteotomy to the right is more suitable for a subcapital fracture and the one to the left to a transcervical neck fracture. Pauwels observed that the obliquity of the fracture line with the horizontal plane significantly affected the prognosis of the fracture.[25] The Pauwels angle is defined as the angle formed by extending the fracture line upwards to meet an imaginary horizontal line drawn on left-right plane and can also be used to predict the best cutting plane for the osteotomy.

2.9 | Prosthesis modeling

To compare the different prosthesis designs, some of the commercially available prosthesis were computationally modeled. The modeling was based on the manufacturers templates and is fully parameterizable, ie, the way the modeling was implemented allows the prosthesis' components dimensioning, so that it is adaptable to the patients' femur dimensions.

Firstly, it is possible to make the size of the femoral stem adaptable to the medullary canal. It is postulated that a cementless hip system consisting of a limited number of femoral components can accommodate the complete range of anatomic cavities. In a cemented hip system, due to the void-filling capacity of the cement layer the number of femoral components that accommodates the whole range of cavity geometries is smaller.[4]

With best femoral stem size estimation, the endosteal broaching is minimized and the most bone mass in the interior walls of the canal is preserved. Hence, the diameter of the medullary canal is calculated along the inferior-superior direction in the perpendicular cross sections. To minimize cavity broaching, the femoral stem component diameter is adjusted to the minimum medullary cavity diameter on the cross sections for uncemented prosthesis and with a minimal tolerance of 2 mm to cemented prosthesis, so that room is left for cement filling.

The prosthesis design also takes in account the measured FNA (Section 2.4) of the patient's femur. Excessively, retroverted or anteverted femurs as well as coxa vara and coxa valga femurs can be compensated in the implant design as the toolbox presented here allows its diagnosis beforehand. Neck preserving stems were added to the implants database as their use requires less bone mass to be removed and therefore minimizes the complications associated with a second THA.[26] Finally, cemented and uncemented prosthesis were also modeled as both fixation methods are in use. In sum, the idea is to have a prosthesis database as broad as possible.

Figure 9 shows 4 examples of modeled prosthesis, together with a photograph of the actual prosthesis for comparison purposes.

2.10 | Prosthesis placement

Loosening is the most common long-term complication following the THA. Moreover, the femoral component

placement and the prosthesis stem design are among the factors that reportedly affect the incidence of loosening. On the other hand, the location of the hip center of rotation substantially affects the load on the hip and the kinematics of the hip joint. Long-term follow-up studies demonstrate significantly higher rates of femoral loosening with acetabular components placed in a superior and lateral (ie, nonanatomic) positions, compared with acetabular components placed in a nearly anatomic position.[27] Another important fact that early studies demonstrate is that 2D prosthesis placement planning is seldom misleading, and therefore, a 3D planning is required for precise prosthetic components relation estimation.[28] Ultimately, there is still debate if acetabular and femoral implants should be orientated in such a way to reconstruct individual anatomy or fit within a safe zone. A recently published paper[29] has shown great variability in native hip joint anatomy, and only a few fitted inside the component orientation criteria known as safe zone. Therefore, the implant placement and sizing will be planned to mimic the native joint anatomy, ie, in such a way that the femoral neck angle, the inclination or version of the femur, and the femoral offset remain unaltered. In cases of femur valgus or varus the prosthetic neck should be adjusted, respectively, reduced and increased, to compensate such abnormalities. Together with orthopedic surgeons, a workflow to restore the center of rotation of the femoral head was implemented and will be described in the following paragraphs.

The fitting problem can be described as finding the set of parameters (translation, rotation, and prosthesis size) that minimize the distance between the input points, strategic on the prosthesis, and the geometrical entity, which is the respective femoral axis in this case. The computational cost of this workflow is very low as it relies merely on algebraic operations with the surface meshes.

The joint reaction force acting on the femoral head is principally oriented in the coronal plane, even though rotational loading for the implant stability also takes an important role; therefore, the characterization of the shape of the endosteal cavity in the anterior-posterior plane is of major importance to implant stability. In this context, the medullary canal can be characterized as normal, stove-piped if they are relatively straight sided and champagne-fluted if they are highly tapered.[4] The shape of the canal is nonproportional to the femoral length, as opposed to neck length or head diameter. Therefore, implants cannot be designed on the basis of an average canal size proportionally scaled for larger and smaller canals in the anatomic range. However, the majority (83%)[4] of the femurs has normal shaped cavities. Consequently, the proposed framework was planned so that it deals with the patient-specific cavity to determine the best prosthesis placement.

Standard femoral stems are designed to extend to the isthmus of the medullary canal (Figure 3) to stabilize component alignment and prevent varus migration. Consequently, selection of an optimal length for components of different size is determined by the relationship between the canal width and depth of the medullary isthmus, which is extremely variable.[4] Hence, it may require intramedullary reaming to broaden the canal which can be considered unnecessary bone mass removal.

On the other hand, studies have shown the importance of a close match between the proximal cross section of the femur and the femoral component.[4] Moreover, stem-bone contact within the metaphysis can only be obtained in discrete areas of the endosteal surface rather than over a substantial portion of the potential interface. For this reason, few femoral components truly fill the femoral canal laterally. In cementless arthroplasties this can lead to excessive micro-motion and impaired clinical performance.

Therefore, the first step of the workflow is to make the interception of the neck and shaft axes of both the femur and the implant coincident and orient the implant according to the prosthesis insertion axis (Figure 3). Then, the stem is scaled so that it is as large as possible with minimal removal of cortical bone from the endosteal. Because only a few predetermined stem sizes are available, the best fit is selected. If the implant stem is smaller than the medullary cavity, there is the risk of prosthesis subsidence, ie, moving inferiorly along the femoral shaft. If, contrarily, the stem is to large for the cavity, the excessive removal of cortical bone can fragilize the load-bearing capacity of the endosteal wall, and ultimately result in a femoral fracture. Moreover, intraoperative femoral fractures have been reported because of wrong stem size estimation. According to our orthopedic partners, the stem and the endosteal wall should have an interference less than 1 mm for uncemented implants to be considered a good fitting. For cemented prosthesis, the workflow takes in account the spacing between the stem and the endosteal wall that it is filled with the cement and a clearance of around 2 mm, depending on the implant model, is left in between the contact surfaces.

Secondly, it is important to maintain the femoral offset, which will ensure that the center of rotation of the joint and leg length are kept unchanged. To do so, the prosthesis is rotated along the insertion axis to minimize the distance to the center of the femoral head. Most prosthesis have a fixed neck angle, so the position of the prosthesis stem is chosen such that the center of the femoral head is mantained in the prosthetic joint. With this alignment, we ensure that the prosthetic center of rotation matches the anatomical center of rotation. In sum, the purpose of the toolbox presented here is to aid the surgical planning and not to undoubtedly determine the optimal size of the prosthesis. It is ultimately the judgment of the surgeon that determines which prosthesis design and size to use in every patient-specific coupling.

3 | RESULTS

The principal component of the singular value decomposition that stands as the direction vector of the FMDA represents

98.1% of the total point cloud scattering that represents the centroids of the cross sections along the femoral shaft. Similarly, the direction vector of the prosthesis insertion axis represents 97.7% of the total variation of the positions of the point cloud.

The sphere fitting to the femoral head was computed by minimizing the distances of the quartic surface that defines the sphere. The average error was 0.42 ± 0.06 mm, which, represents less than 1% of the average 46.1 ± 4.8 mm diameter of the femoral head.[4]

In this section, some examples of the uses of the set of numerical methods here presented are shown. Figure 10 shows an example of a fitting of a TRI-LOCK® Bone Preservation Stem to a patient-specific femur.

It is ensured that the head center lies within the axis of the implant neck with the proposed sizing and fitting. In this specific patient, the femoral head would be inserted halfway in the neck so that the center of the femoral head remains unchanged in the prosthetic joint. Moreover, due to the flattened nature of the stem in the anterior-posterior direction, most fitting to the endosteal is done in the coronal plane.

A second example of an uncemented prosthesis is illustrated in Figure 11, where the sizing and fitting of a VerSys Epoch® FullCoat Hip System is shown. Intuitively, we can verify the good sizing of the implant stem to promote maximum contact surface in the endosteal wall. With a fixed implant-shaft neck angle it is important also to ensure that the femoral head center lies within the neck axis of the implant, both frontally and sagittally.

Figure 12 shows the MS-30™ cemented prosthesis, automatically sized and placed in a generic femur so that the implant size trial and error is avoided in the surgical intervention.

As is observed in Figure 12 the prosthesis fitted significantly well. The tip of the stem was placed at the medullary isthmus and the rotation center of the hip center is maintained, as the prosthetic hip rotation center is maintained. Although the stem fits the femoral walls in the frontal plane, its flattened design can be seen in the lateral views. This is because the MS-30™ is a cemented stem and space needs to be taken in account for the cement filling.

Finally, an example of a fitting of a neck preserving implant achieved with the proposed toolbox is illustrated in Figure 13.

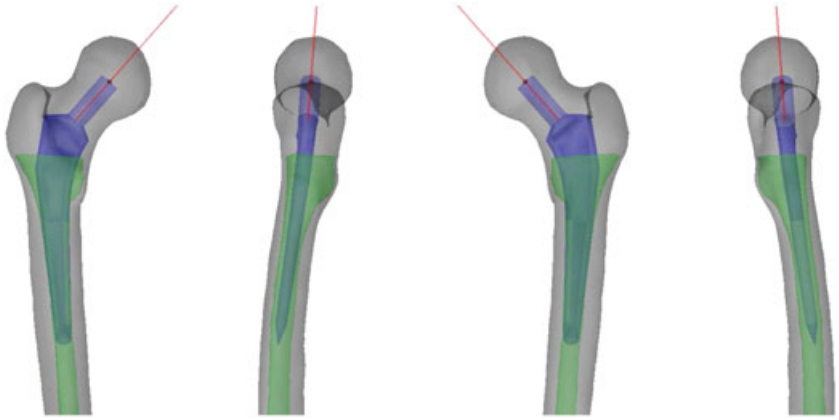

FIGURE 10 From left to right: posterior, left, anterior, and right views of an example of a DePuy Synthes TRI-LOCK® implant fitting to a patient-specific femur. The femur is represented in translucent black with the center of the femoral head in black. The implant and the medullary cavity are shown in blue and green, respectively. In red, the prosthesis neck axis is visible

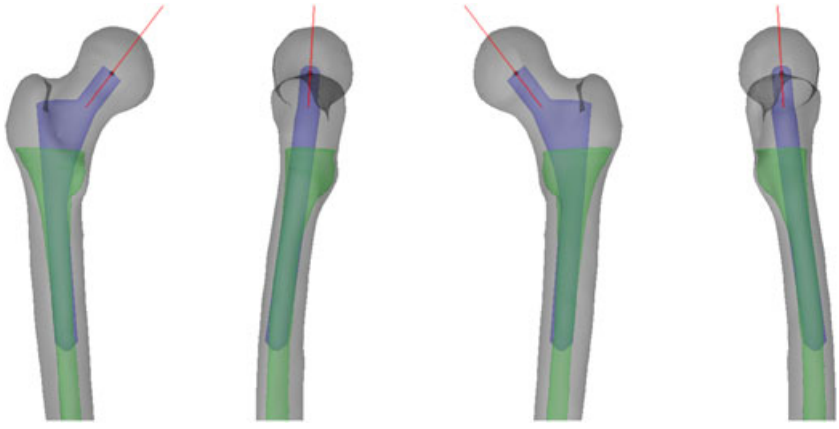

FIGURE 11 From left to right: posterior, left, anterior, and right views of an example of a VerSys Epoch® FullCoat Hip System fitting to a patient-specific femur. The femur is represented in translucent black with the center of the femoral head in black. The implant and the medullary cavity are shown in blue and green, respectively. In red, the prosthesis neck axis is visible

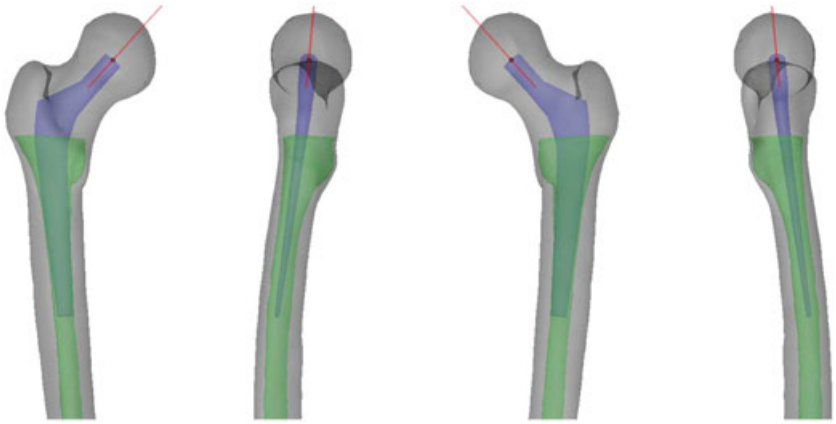

FIGURE 12 From left to right: posterior, left, anterior and right views of an example of a Zimmer® MS-30™ implant fitting to a patient-specific femur. The femur is represented in translucent black with the center of the femoral head in black. The implant and the medullary cavity are shown in blue and green, respectively. In red, the prosthesis neck axis is visible

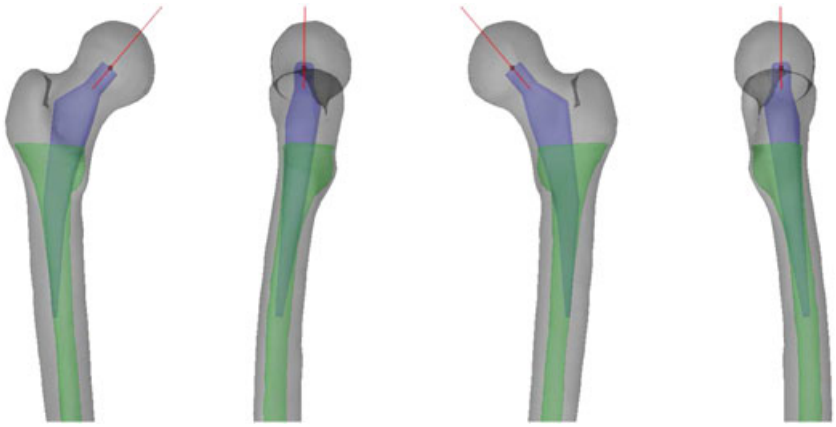

FIGURE 13 From left to right: posterior, left, anterior and right views of an example of a Zimmer® Mayo® implant fitting to a patient-specific femur. The femur is represented in translucent black with the center of the femoral head in black. The implant and the medullary cavity are shown in blue and green, respectively. In red, the prosthesis neck axis is visible

The Mayo® Conservative Hip Prosthesis has a shortened distal stem that fixates distally against the lateral endosteal wall that promotes minimal cortical bone removal, which is one of the most determinant factors in a revision surgery. Due to that reason, the orientation of the prostheses stem axis is done accordingly and not as the previous examples have been shown.

As Figures 10 to 13 show, the alignment and sizing is in conformity with the workflow described in the Section 2.10. The prosthesis' stem is aligned according to the prosthesis insertion axis, and its size is fitted to the endosteal of the medullary cavity. This way the contact between the stem and the endosteal is maximized and the mechanical stresses at the bone-implant interface are potentially reduced.

Moreover, it is also observable that the prostheses are aligned with the FNA. This led to the minimization of the distance between the tip of the implant neck and the center of rotation of the femur. The distance between the tip of the femoral neck and the center of the femoral head is usually compensated by the configuration of the prosthetic head as the insertion socket can have controlled depth so that ultimately the femoral offset and leg length remain unchanged in the prosthetic configuration.

4 | DISCUSSION

Firstly, not only the linear regression of the FMDA and the prosthesis insertion axis but also the sphere fitting of the femoral head were performed accurately, ie, presenting very low error values. Automatic 3D axes are therefore established for prosthesis insertion axis and take in account femoral anteversion or excessive retroversion in implant positioning, which is hard to achieve based in radiographic templating alone.

The values found for the neck-shaft and anteversion angles corroborate other values found in the literature.[4,24] The proposed methodology can easily be adapted to diagnose femur valgus or vara and retroverted or excessively anteverted femurs merely by measuring the angles between the defined axes. In presurgical planning this allows the surgeon to correct the femur anteversion during the THA and potentially prevent future hip complications on the patient.

Overall, the landmark extraction is achieved within a few seconds, as it only relies on geometric transformations in its majority, which are computationally very efficient. This is of critical importance when implemented in an interactive software where the surgeon is planning the THA. The methodology was able to accurately predict landmark location as well as estimate the axis and the angles above described for all of the 50 bone models, which stands as proof of the methods' repeatability and user independence. The accuracy error is inherent to the segmentation error and the coarsening and smoothing of the surface mesh, which are beyond the incidence of the present study. It is however possible to implement mesh refinement in more detailed regions of the femur, eg, the trochanters, to minimize the accuracy error.

The prosthesis placement workflow firstly ensured an accurate implant head rotation center reconstruction. Then, by orienting the implant neck as to mimic the anatomical FNA, femoral retroversion and excessive femoral anteversion can be previously measured so that the surgeon can place the implant to compensate these deviations. The femoral stem fixation to the endosteal is done by aligninging the stem axis with the prosthesis insertion axis. The sizing of the implant is done such that the interference or clearance distance is in agreement with the surgeon's opinion. To do so, an interactive user interface is provided for the doctor to test or even to question the workflow's suggestion. This way the prosthesis subsidence is minimized even in cementless stems.

An experienced orthopedic surgeon can indeed achieve similar results to any of the 4 examples shown in Section 3, at the cost of time and on the basis of his experience and expertise. Hence, a positive clinical feedback relative to the implant dimensioning and positioning was given by the partner surgeon, because the developed workflow promotes a good fixation of the stem as well as a good implant neck orientation. This ensures that the offset remains unaltered, and consequently, equal leg length is maintained. The lateralization of the center of rotation directly influences the lever arm of abductor muscles, which play an important part during the gait cycle and can result in a defective gait cycle, ie, limping. The restoration of the hip center of rotation can decrease the incidence of failures and reduce the need for revision surgery.[24] On the other hand, our method can be improved by fully mapping the cancelous and cortical bone boundaries. With so, a more accurate representation of the bone tissue's properties can be achieved, considering the bone mass density.

The work here presented is limited by the amount of different modeled prosthesis. Recent approaches to hip replacement implants, namely, geometries and coatings, have been developed and have not yet been used to test this workflow. Moreover, there are other optimization criteria that also need to be in agreement with the planning here, such as leg length and the femoral offset. In fact, while restoring the center of the head in a clinical environment, there is often the need to adjust its position as to correct leg length discrepancy or offset differences, which is not still taken in account in the presented planning toolbox. Implants have various but limited sizes available, hence emphasizing the importance of the surgeon's final decision on which size is better suitable for one given femoral geometry, regardless the present workflows suggestion. It should be also noticed that landmark extraction depends on the bone surface mesh level of detail. However, if the same segmentation process is used for every surface mesh, the same data point structure is kept, even in low-resolution CT scans.[22] Future improvements should also take in account acetabular component sizing and placement as well as look to mantain the biomechanics of the prosthetic joint as close to the anatomical joint as possible. Comparative leg lengths between legs are yet another limitation of this work and future work should consider the hypothesis of leg lenghts need to be corrected.

To the author's knowledge, there is only 1 report of fully automated optimization methods of preoperative THA planning on the basis of computational anatomy.[30] The approach is formulated as maximum a posterior estimation on the basis of statistical models derived from the training datasets prepared by a surgeon. The results shown are satisfactory and are said to improve the surgeon's planning. Nevertheless, if, on the one hand, the training of the shape model can be time consuming, an approach on the basis of shape models might incorporate the errors of femur-prosthesis couplings population. The approach considers also the acetabular component of the hip implant which makes results quite difficult to compare.[31]

5 | CONCLUSIONS

Even though the reduction of the incidence of hip implants failure on THA to zero is still difficult to achieve, the developed set of tools is a step forward toward better planning and hopefully to increase the longevity of the implants. The automated landmark extraction and consequent anatomical knowledge of the patient-specific femur allows an accurate and straightforward planning from the surgeon who, due to the automation of most of these methods, does not need to have extensive knowledge of the implemented numerical methods. An accurate prosthesis sizing, fitting, and placement can increase the precision of the surgery, shorten its duration and cost and reduce the incidence of prosthesis' loosening and minimize bone stock loss, which will ultimately influence the terms of a possible revision surgery. Moreover, by maintaining equal head rotation centers and if leg length is ensured to be kept unaltered, the risk of periprosthetic fracture is minimized as well as a normal gait cycle is more likely to be restored. In sum, a good planning reduces the risk of major errors but does not guarantee the everlasting success of a THA.

Within the scope of this paper, the methods here presented were tested on 50 femur models. They proved to be both robust, precise, and repeatable. The automated workflow

developed can also be coupled to an automatic finite element model to infer quantitative data of a specific implant-femur coupling, which can be used to presurgically compare the performance of different implant designs.

ACKNOWLEDGMENTS

This work was funded by FEDER through the operational program Competitiveness Factors COMPETE. This work was also supported by the Portuguese Foundation for Science and Technology (FCT), project PTDC/SAU-BEB/103408/2008 and scholarship SFRH/BD/71822/2010, and through IDMEC, under LAETA, project UID/EMS/50022/2013.

REFERENCES

1. Holszarth U, Cotogno G. Total hip arthroplasty—state of the art, challenges and prospects. *European Commission Joint Research Centre*, Luxembourg; 2012.
2. Eggli S, Pisan M, Mller ME. The value of preoperative planning for total hip arthroplasty. *J Bone Joint Surg Br*. 1998;80(3):382–390.
3. Maruyama M, Feinberg JR, Capello WN, D'Antonio JA. Morphologic features of the acetabulum and femur: anteversion angle and implant positioning. *J Clin Orthop Relat Res*. 1994;393:52–65.
4. Noble PC, Alexander JW, Lindahl LJ, Yew DT. The anatomic basis of femoral component design. *J Clin Orthop Relat Res*. 1988;235:148–165.
5. Goyal N, Stulberg SD. Evaluating the precision of preoperative planning in patient specific instrumentation: can a single MRI yield different preoperative plans? *J Arthroplasty*. 2015;30(7):1250–1253.
6. Lattanzi R, Baruffaldi F, Zannoni C, Viceconti M. Specialised CT scan protocols for 3-D pre-operative planning of total hip replacement. *Med Eng Phys*. 2004;26(3):237–245.
7. Jan SVS, Sobzack S, Dugailly PM, et al.. Low-dose computed tomography: a solution for in vivo medical imaging and accurate patient-specific 3D bone modeling? *Clin Biomech*. 2006;21(9):992–998.
8. Goo HW. CT radiation dose optimization and estimation: an update for radiologists. *Korean J Radiol*. 2012;13(1):1–11.
9. Noble PC, Nobuhiko S, Johnston JD, et al.. Computer simulation: how can it help the surgeon optimize implant position? *J Clin Orthop Relat Res*. 2003;417:242–252.
10. Cheng E, Chen J, Yang J, et al. Automatic Dent-landmark detection in 3-D CBCT dental volumes. *J Engineering in Medicine and Biology Society, EMBC, 2011 Annual International Conference of the IEEE*; 2011:6204–6207.
11. Moos S, Marcolin F, Tornincasa S, et al. Cleft lip pathology diagnosis and foetal landmark extraction via 3D geometrical analysis. *Int J Interactive Design and Manufacturing*. 2014:1–18.
12. Röling MA, Visser MI, Oei EHG, Pilot P, Kleinrensink GJ, Bloem RM. A quantitative non-invasive assessment of femoroacetabular impingement with CT-based dynamic simulation-cadaveric validation study. *BMC Musculoskelet Disord*. 2015;16:50. doi:10.1186/s12891-015-0504-7
13. Van Cauter S, De Beule M, Van Haver A, Verdonk P, Verhegghe B. Automated extraction of the femoral anatomical axis for determining the intramedullary rod parameters in total knee arthroplasty. *Int J Numer Method Biomed Eng*. 2012;28:158–169.
14. Yun JS, Lee YS, Jung JJ, et al. The Zuckerkandl's tubercle: a useful anatomical landmark for detecting both the recurrent laryngeal nerve and the superior parathyroid during thyroid surgery. *Endocr J*. 2008;55(5):925–930.
15. Hajeer MY, Ayoub AF, Millett DT, Bock M, Siebert JP. Three-dimensional imaging in orthognathic surgery: the clinical application of a new method. *Int J Adult Orthodon Orthognath Surg*. 2001;17(4):318–330.
16. Wrobel K, Stevens SR, Jones RH, et al. A landmark analysis of 30-day mortality after coronary artery bypass surgery in patients with ischemic heart failure: Results of the surgical treatment for ischemic heart failure (STICH) trial. *J Circulation*. 2014;130(Suppl 2):A19392.
17. Nicola Mondanelli, Giron F, Losco M, Buzzi R, Aglietti P. Opening wedge high tibial osteotomy using a monoaxial dynamic external fixator. *Knee Surgery, Sports Traumatology, Arthroscopy*. 2015. doi:10.1007/s00167-015-3564-1.
18. EBeil W, Rohr K, Stiehl HS. Investigation of approaches for the localization of anatomical landmarks in 3D medical images. *Proc. Computer Assisted Radiology and Surgery CAR*. 1997;97:25–28.
19. Baek SY, Wang JH, Song I, Lee K, Lee J, Koo S. Automated bone landmarks prediction on the femur using anatomical deformation technique. *J Computer-Aided Design*. 2013;45(2):505–510.
20. Ehrhardt J, Handels H, Strathmann B, Malina T, Plötz W, Pöppl SJ. Atlas-based recognition of anatomical structures and landmarks to support the virtual three-dimensional planning of hip operations. In *Medical Image Computing and Computer-Assisted Intervention-MICCAI 2003*. Springer 2003:17–24.
21. Subburaj K, Ravi B, Agarwal M. Automated identification of anatomical landmarks on 3D bone models reconstructed from CT scan images. *Comput Med Imaging Graph*. 2009;33(5):359–368.
22. Almeida DF, Ruben RB, Folgado J, Fernandes PR, De Beule M, Verhegghe B. Fully automated segmentation of femurs with medullary canal definition for low resolution CT scans. *Med Eng Phys*. 2015. doi:10.1016/j.medengphy.2016.09.019.
23. Viste A, Trouillet F, Testa R, Chèze L, Desmarchelier R, Fessy MH. An evaluation of CT-scan to locate the femoral head centre and its implication for hip surgeons. *J Surg Radiol Anat*. 2014;36(3):259–263.
24. Lecerf G, Fessy MH, Philippot R, et al. Femoral offset: anatomical concept, definition, assessment, implications for preoperative templating and hip arthroplasty. *Orthop Traumatol Sur*. 2009;95(3):210–219.
25. Bartonícek J. Pauwels' classification of femoral neck fractures: correct interpretation of the original. *J Orthopaedic Trauma*. 2001;15(5):358–360.
26. Röhrl SM, Li MG, Pedersen E, Ullmark G, Nivbrant B. Migration pattern of a short femoral neck preserving stem. *Clin Orthop Relat Res*. 2006;448:73–78.
27. Yoder SA, Brand RA, Pedersen DR, O'Gorman TW. Total hip acetabular component position affects component loosening rates. *Clin Orthop Relat Res*. 1988;288:79–87.
28. Herrlin K, Pettersson H, Selvik G. Comparison of two-and three-dimensional methods for assessment of orientation of the total hip prosthesis. *Acta Radiologica*. 1988;29(3):357–361.
29. Merle C, Grammatopoulos G, Waldstein W, et al. Comparison of native anatomy with recommended safe component orientation in total hip arthroplasty for primary osteoarthritis. *J Bone Joint Surg*. 2013;95(22):e172.
30. Kagiyama Y, Takao M, Sugano N, Tada Y, Tomiyama N, Sato Y. Optimization of surgical planning of total hip arthroplasty based on computational anatomy. *2013 35th Annual International Conference of the IEEE Eng Med Biol Soc (EMBC)*. 2013;95(22):2980–2983.
31. Ruben RB, Folgado J, Fernandes PR. Three-dimensional shape optimization of hip prostheses using a multicriteria formulation. *Struct Multidiscipl Optim*. 2007;34(3):261–275.

How to cite this article: de Almeida DF, Ruben RB, Folgado J et al. Automated femoral landmark extraction for optimal prosthesis placement in total hip arthroplasty. *Int J Numer Meth Biomed Engng*. 2017;33:e2844. https://doi.org/10.1002/cnm.2844